American Mineralogist, Volume 89, pages 1772–1783, 2004

Epidote-rich talc-kyanite-phengite eclogites, Sulu terrane, eastern China: *P-T-f*$_{O_2}$ estimates and the significance of the epidote-talc assemblage in eclogite

CHRISTOPHER G. MATTINSON,* RU Y. ZHANG, TATSUKI TSUJIMORI, AND JUHN G. LIOU

Department of Geological and Environmental Sciences, Stanford University, Stanford, California 94305-2115, U.S.A.

ABSTRACT

Eclogites interlayered with gneiss and minor quartzite in the Qinglongshan near Donghai are characterized by unusually abundant (15–40 vol%) hydrous phases including talc, phengite, and epidote; many also contain kyanite. Garnet hosts both prograde (paragonite, amphibole, epidote) and peak stage (omphacite, epidote, phengite, kyanite) mineral inclusions. Several eclogites contain talc rimmed by barroisite; optically and compositionally similar coarse-grained amphibole in other samples indicates that the reaction Omp + Tlc = Amp has completely consumed talc. Estimated peak conditions of 30–35 kbar, 600–700 °C, are consistent with polycrystalline quartz pseudomorphs after coesite included in garnet, omphacite, epidote, and kyanite, and up to 3.6 Si pfu (11 O atom basis) in phengite. Garnet-epidote oxygen barometry on the peak metamorphic assemblage indicates oxygen fugacities above the Hem-Mag buffer, consistent with the epidote + talc assemblage and 5–20 mol% aegerine component in omphacite. The high oxygen fugacity calculated in this study as well as previously documented negative oxygen isotope values recorded by these rocks may both reflect alteration by oxidizing, meteoric water in a hydrothermal system. Oxidized conditions during peak metamorphism may explain the extreme scarcity of microdiamond in this area. The Ep + Tlc assemblage is stabilized by high oxygen fugacity, and demonstrates that talc-bearing eclogites are not restricted only to unusually Mg-rich bulk compositions.

INTRODUCTION

Ultrahigh-pressure (UHP) metamorphic rocks are a volumetrically minor but petrotectonically significant feature of continental collision zones. Discovery of metamorphic coesite (Chopin 1984; Smith 1984) and diamond (Sobolev and Shatsky 1990) provided the first unambiguous evidence for the return to the surface of deeply subducted (>80–120 km) crustal rocks. Subsequent studies have discovered UHP metamorphism in more than a dozen localities (for summary, see Liou et al. 2002). Although eclogites and garnet peridotites typically best preserve mineralogic evidence for UHP metamorphism, index minerals (coesite, diamond) included in garnet and zircon from felsic gneisses at many UHP localities (e.g., Chopin 1984; Katayama et al. 2002; Liu et al. 2001, 2002; Sobolev and Shatsky 1990; Ye et al. 2001) demonstrate that km-scale tracts of felsic gneiss have recrystallized under UHP conditions and were exhumed together with mafic/ultramafic rocks. The buoyancy of the volumetrically dominant felsic rocks probably allowed the transport of the dense mafic/ultramafic rocks to the surface (e.g., Ernst et al. 1997).

This paper describes samples from the Qinglongshan, near Donghai, in the Sulu UHP terrane of eastern China (Fig. 1). Eclogites typically contain abundant hydrous phases including talc, phengite, and epidote. The continuous exposure on a highway roadcut reveals that the section of interlayered gneiss, eclogite, and minor quartzite is coherent, cut only by a few minor faults (Fig. 2). Petrography, mineral chemistry, and estimates of pressure, temperature, and oxygen fugacity were conducted to constrain formation conditions of these rocks, and to examine the significance of the epidote-talc assemblage in eclogite.

GEOLOGIC SETTING

The Dabie-Sulu UHP belt in eastern China (Fig. 1) is the result of Triassic subduction and collision of the Yangtze craton to the south beneath the Sino-Korean craton to the north. Proterozoic (?) basement and the Upper Proterozoic passive margin sequence of the Yangtze craton recrystallized under UHP conditions, and studies in the Dabieshan indicate that exhumation to mid-crustal levels from depths of at least 120 km occurred in the Middle to Late Triassic (Hacker et al. 2000). Initial surface exposure of HP-UHP rocks occurred in the Middle Jurassic to Early Cretaceous (Ratschbacher et al. 2000; Grimmer et al. 2003). The Dabie and Sulu UHP belts are separated by 500 km of left-lateral offset on the post-Triassic Tan Lu fault (Rumble et al. 2002).

Low mineral and bulk-rock oxygen and hydrogen isotope values measured in a large (>50 km × 50 km) area near Qinglongshan (Yui et al. 1995; Rumble and Yui 1998; Rumble et al. 2002; Zheng et al. 2003) and in Dabieshan (Baker et al. 1997; Zheng et al. 2003) suggest that the protoliths of these rocks interacted with meteoric water during a period of cold climate, and preserved their anomalously low isotopic signature during subsequent UHP metamorphism. Zircon U-Pb geochronology and oxygen isotope analyses from metagranites near Qinglongshan indicate that the low isotopic values were acquired during hydrothermal activity accompanying Late Proterozoic granite intrusion, at approximately the same time as the Sturtian ("snowball earth") glacial episode (Rumble et al. 2002; Zheng et al. 2003).

Our study area is in the southeastern part of the Sulu UHP belt, near Donghai in eastern China (Fig. 1). Coesite and coesite pseudomorphs occur in both eclogite and felsic gneiss throughout the Sulu terrane in surface exposures as well as drill core samples to depths of 200–1028 m (Zhang et al. 1995a; Liu et al. 2001, 2002). Previous studies in the Donghai region have documented eclogite with hydrous phases including talc, epidote minerals, and phengite (Zhang et al. 1995a), and OH-rich topaz from kyanite quartzites (Zhang et al. 2002). Exposure of UHP

* E-mail: cgm@pangea.stanford.edu

0003-004X/04/1112–1772$05.00

rocks is typically poor in the Sulu terrane, but a continuous 660 m section across the Qinglongshan exposed concordant gneiss, eclogite, and minor quartzite (Fig. 2), permitting collection of fresh samples. Eclogite layers are concordant with gneissic rocks and quartzites; a few boudins have discordant contacts. The foliation strikes 020–040° and dips 45–65° SE, and the section is cut by several minor, high-angle faults.

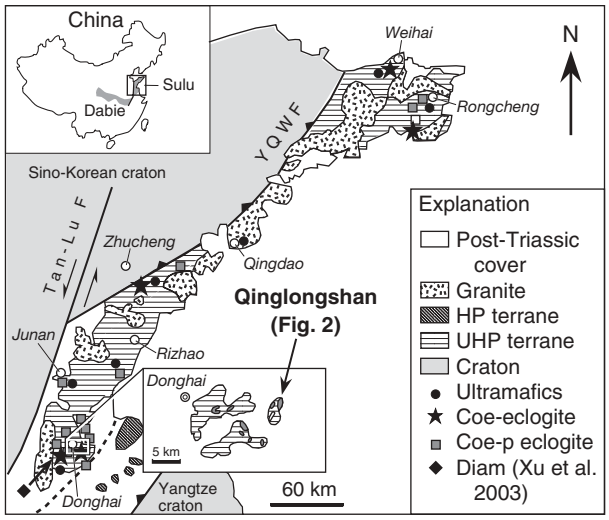

FIGURE 1. Geologic sketch map of the Sulu region showing major tectonic units, distribution of coesite-bearing eclogite (Coe-eclogite) and coesite pseudomorph-bearing eclogite (Coe-p eclogite). White circles mark the location of labelled towns. YQWF, Yantai-Qingdao-Wulian fault (after Zhang et al. 2002).

PETROGRAPHY

Eclogite

Eclogites are foliated to massive and are medium- to coarse-grained (0.2–5 mm). Amphibolite-facies retrogression is variable but generally minor. Mineral assemblages and modal abundances are summarized in Table 1, and representative photomicrographs and back-scattered electron (BSE) images are shown in Figures 3 and 4. Mineral abbreviations follow Kretz (1983) except amphibole (Amp), coesite (Coe), coesite pseudomorph (Coe-p), phengite (Phe), and as noted. Eclogites typically contain the peak assemblage Grt + Omp + Ky + Ep + Phe + Rt + Coe/Qtz ± Tlc, except for one eclogite (QL6B), which lacks epidote, kyanite, talc, and quartz. In addition to common inclusions of rutile, phengite, and omphacite, the centers of garnets from several samples contain sparse inclusions of paragonite, epidote, and amphibole (Figs. 4a and 4b). These inclusions are similar to prograde inclusions reported in the Sulu terrane (Enami and Nagasaki 1999; Wallis et al. 2000; Zhang et al. 1995a) and in western Norway (e.g., Krogh 1982). Most omphacite grains exhibit optically distinct cores that contain thin (<2 μm) quartz (?) exsolution rods. Quartz rods reported from other UHP localities (for sum-

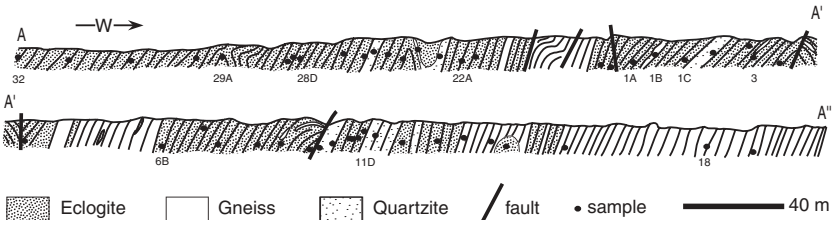

FIGURE 2. Cross section across the Qinglongshan (location shown in Fig. 1); numbers indicate samples discussed in the text (QL prefix omitted). The foliation strikes 020–040° and dips 45–65° SE. Vertical exaggeration ~5×.

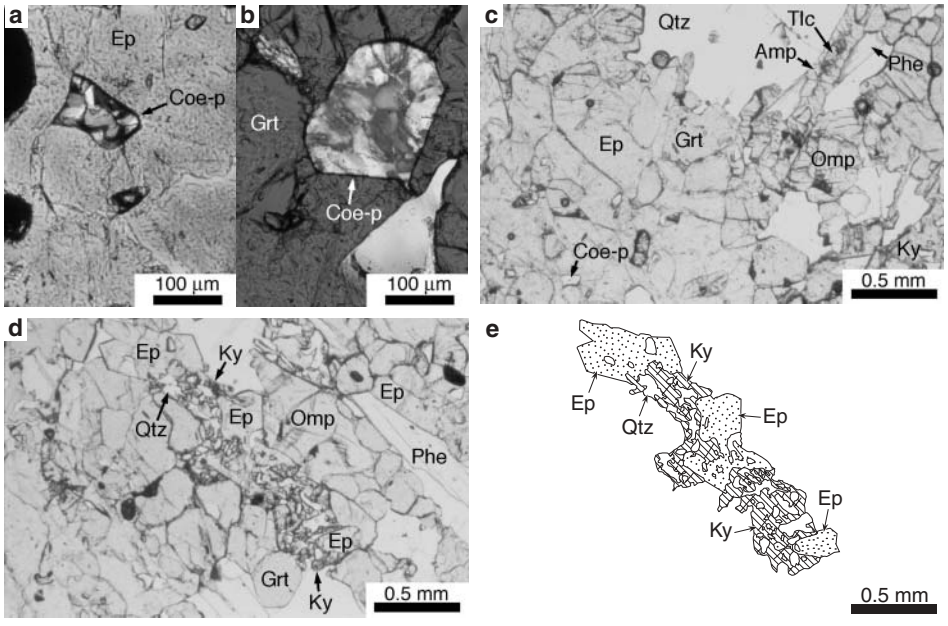

FIGURE 3. Photomicrographs: (**a**) Coesite pseudomorph (Coe-p) in Ep II poikiloblast. Sample QL3, crossed polarizers. (**b**) Coesite pseudomorph (Coe-p) in garnet. Sample QL28D, crossed polarizers, gypsum plate inserted. (**c**) Talc rimmed by amphibole cross cuts phengite; Ep II poikiloblast fills left side of photo, and contains garnet and omphacite inclusions and coesite pseudomorph (Coe-p) (enlarged view shown in **a**); Ky II is intergrown with quartz. Sample QL3, plane polarized light. (**d**) Ep III and Ky II mutually intergrown with quartz. Sample QL1A, plane polarized light. (**e**) Sketch of (**d**) illustrating Ep III-Ky II-Qtz intergrowth. Note vermicular intergrowth of quartz (unpatterened) with kyanite (ruled) and epidote (stippled).

TABLE 1. Eclogite modal abundances

Sample no.	Grt	Ky I	Ky II	Ep I	Ep II	Ep III	Ep IV	Omp	Amp I	Amp II	Amp III	Phe	Pg	Tlc	Ab	Qtz/Coe	symplectite
QL1A	30	2–3	1		20	5		20		10		5				5	1–2
QL1C	15	3			20	5	5	2			10	<1			5	10	30
QL3	30	1–2	2–3	<1	25–30	5		10	<1	5–10		2–3	<1	<1		5	1–2
QL6B	35							50		<1		10					
QL22A	25	1	<1		15	5		25	<1	15		3	<1			5	2
QL28D	20	<1	1		5	20		20	<1	15		1–2	<1	<1		15	1
QL29A	20	<1	5		15	15		30	<1	15		3–5		1–2		3–5	1–2
QL32	30	<1	3		10	3		35	<1	5–10		5	<1	1–2		3	1

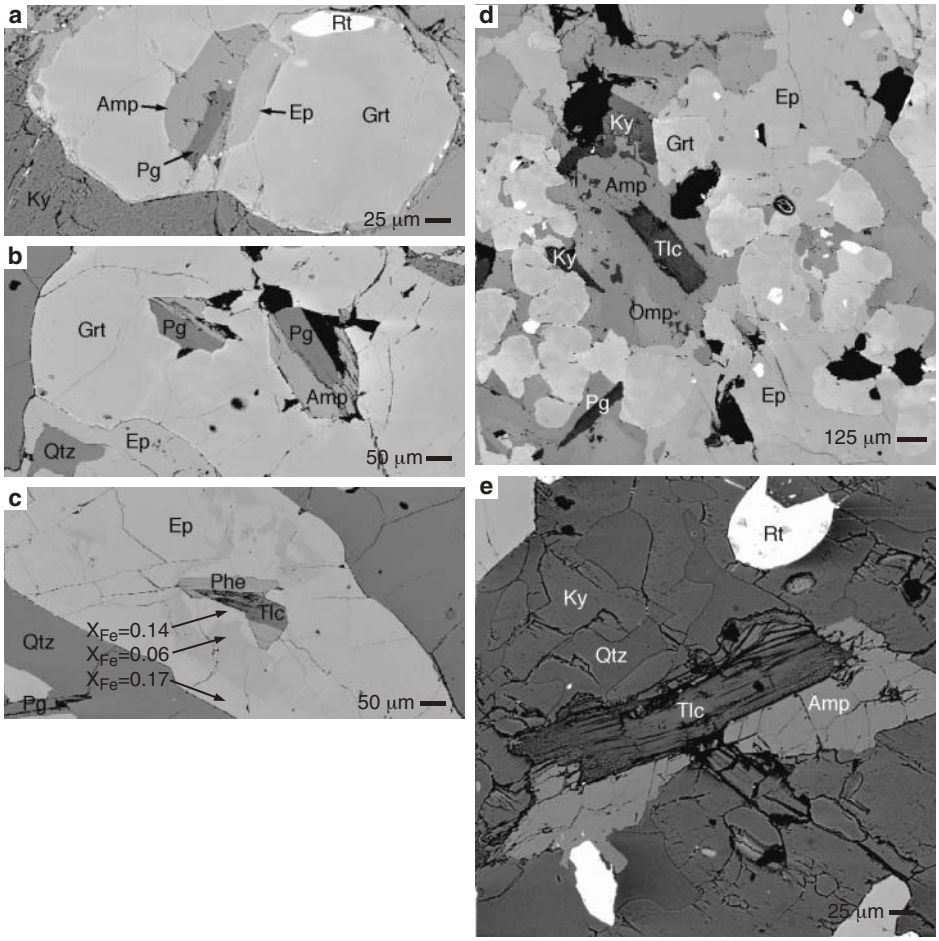

FIGURE 4. Back scattered electron images (brightness is proportional to average atomic number): (**a**) Pg + Amp I + Ep I compound inclusion in garnet, sample QL3. (**b**) Pg + Amp I compound inclusions in garnet, sample QL28D. (**c**) Tlc + Phe compound inclusion within Ep I/II?, sample QL28D. This epidote is unlike any of the stages present in the other samples. The dark, medial region corresponds to the Fe-poorest compositions plotted in Figure 6. (**d**) Talc breakdown texture, sample QL32. Amp II partially replaces talc and omphacite (for compositional zoning of amphibole, see Fig. 8). Retrograde paragonite cuts amphibole (for composition see Fig. 9). Ep II encloses garnet. (**e**) Talc partially rimmed by Amp II included within Ky II poikiloblast, sample QL32. Note the irregular intergrowth of Ky II and quartz: kyanite is slightly brighter than quartz, and pits from polishing and cleavage cracks are faintly visible in kyanite, in contrast to the smooth surface of quartz.

mary, see Zhang and Liou 2000) are interpreted to result from the breakdown of the super-silicic clinopyroxene stabilized by UHP conditions. Most samples contain several texturally distinct generations of epidote. Epidote inclusions (Ep I) occur only in garnet and omphacite, in some cases as compound inclusions with amphibole ± paragonite (Fig. 4a). Large epidote poikiloblasts (Ep II) enclose garnet, omphacite, and quartz (including coesite pseudomorphs; Figs. 3a and 3c). Skeletal epidote (Ep III) contains a vermicular intergrowth of optically continuous quartz but lacks coesite pseudomorphs (in some samples Ep III is also intergrown with kyanite; Figs. 3d and 3e). Epidote rims and new grains (Ep IV) richer in Fe (see below) are restricted to extensively amphibolitized samples. Some of the epidote grains are aligned with the foliation defined by omphacite and phengite, but most poikiloblasts cross cut it. One epidote grain contains a compound Phe + Tlc inclusion and an Fe-poor medial zone (sample QL28D, Fig. 4c), unlike any of the epidote stages recognized in the other samples. The patchy zoning of this grain suggests that an Fe-poor epidote was partially replaced by an Fe-rich composition similar to the Ep II and Ep III grains in the other samples. Amphibole is present as inclusions in garnet and omphacite (Amp I), large blue-gray barroisite poikiloblasts (Amp II; Leake et al. 1997 amphibole classification), and extensively amphibolitized samples also contain green pargasite (Amp III), which forms both new grains and rims around barroisite (Amp II). Fine-grained amphibole is also present in the symplectite surrounding garnet and omphacite. The phengite grains are primarily aligned with the foliation, but some grains cut the foliation, suggesting more than one stage of growth. Paragonite occurs as inclusions in garnet, and as late-stage neoblasts in the matrix (Figs. 4a–4d). Rutile contains ubiquitous red lamellae (Ti-hematite?), incipiently replaced by ilmenite in fresh samples,

and extensively replaced by an intergrowth of ilmenite + Ti-hematite (?) in retrogressed samples. Kyanite porphyroblasts in most samples (up to 5 vol%) are present as subidioblastic or rounded grains with rare inclusions of quartz (Ky I) ±large irregular grains (Ky II) with a vermicular intergrowth of abundant quartz (±Ep±Grt; Figs. 3c–3e and 4e). Several samples contain irregular inclusions of Ky I in mica (Pg?), suggestive of a reaction relationship. A rim of "palisade" albite is developed at the boundary between kyanite and quartz in extensively retrogressed samples, probably representing a reaction such as Ky + Qtz + Na (from Omp) = Ab. Talc rimmed by pale blue-gray barroisite (Amp II) occurs in several samples (Figs. 3c, 4d, and 4e), and the presence of similar coarse-grained amphibole in other samples suggests that the reaction Omp + Tlc = Amp has completely consumed pre-existing talc. A symplectite of plagioclase, sodic augite, and amphibole occurs along omphacite grain boundaries in most eclogites; symplectite replaces omphacite completely, and garnet partially, in extensively retrogressed samples. Quartz (up to 20 vol%) occurs as irregular grains in the matrix, and as single or polycrystalline inclusions in other minerals. Polycrystalline quartz inclusions probably representing coesite pseudomorphs occur in garnet, epidote, kyanite, and omphacite (Figs. 3a and 3b), but relict coesite is absent.

TABLE 2A. Eclogite garnet compositions

Sample	QL6B-c	QL22A-c	QL22A-r	QL32
Analysis	1	2	3	4
SiO_2	39.46	38.99	39.10	40.90
Al_2O_3	22.57	21.96	22.00	22.54
Fe_2O_3	0.55	1.31	1.94	–
FeO	20.99	20.95	17.75	17.90
MnO	0.41	1.12	0.79	0.47
MgO	8.31	8.62	11.10	12.60
CaO	8.55	7.16	6.50	6.17
Totals	100.86	100.12	99.18	100.59
Si	2.980	2.975	2.963	3.022
Al	2.009	1.975	1.966	1.963
Fe^{3+}	0.031	0.075	0.111	–
Fe^{2+}	1.326	1.337	1.125	1.106
Mn	0.026	0.072	0.051	0.030
Mg	0.936	0.980	1.254	1.387
Ca	0.693	0.586	0.528	0.489
Sum	8.000	8.000	8.000	7.997

Notes: Formulae calculated for 12 O atoms. Abbreviations: c = core; r = rim.

TABLE 2B. Epidote compositions

Sample	QL1A-r	QL1A-r	QL1B-r	QL1C-r	QL3-i	QL22A-r	QL28D	QL32-r
Rock	eclogite	eclogite	gneiss	eclogite	eclogite	eclogite	eclogite	eclogite
Note	Ep II	Ep III		Ep IV	Ep I	Ep II	Ep I/II?	Ep II
Analysis	1	2	3	4	5	6	7	8
SiO_2	38.43	38.32	36.52	37.64	37.56	38.40	39.27	38.43
TiO_2	0.08	0.07	–	0.14	–	0.11	–	–
Al_2O_3	26.92	26.12	21.05	23.79	24.31	27.60	30.22	26.77
Fe_2O_3	7.64	9.03	15.03	12.42	13.12	8.00	2.96	9.46
MnO*	–	–	1.10	0.16	0.16	0.16	–	0.07
MgO	0.37	0.23	–	0.10	0.20	0.30	0.21	0.22
CaO	22.58	22.22	20.71	22.94	22.04	23.20	23.77	23.17
Totals	96.02	95.99	94.43	97.21	97.42	97.79	96.46	98.14
Si	3.039	3.043	3.036	3.007	2.990	2.994	3.044	3.000
Ti	0.005	0.004	–	0.008	–	0.006	–	–
Al	2.510	2.445	2.063	2.241	2.282	2.537	2.761	2.464
Fe^{3+}	0.454	0.539	0.940	0.747	0.786	0.469	0.173	0.556
Mn	–	–	0.077	0.011	0.011	0.011	–	0.005
Mg	0.044	0.027	–	0.012	0.024	0.035	0.024	0.026
Ca	1.914	1.891	1.846	1.966	1.882	1.940	1.976	1.940
Sum	7.966	7.950	7.963	7.991	7.976	7.993	7.979	7.990

Notes: Formulae calculated for 12.5 O atoms. Abbreviations: c = core; r = rim; i = inclusion; MnO* = total Mn as MnO.

Quartzite and gneiss

Polygonal quartz and plagioclase ± K-feldspar surround foliation-defining muscovite, skeletal, strongly zoned epidote, minor euhedral garnet, and titanite. Opaque grains (Ti-hematite) are present both as rims around titanite and as separate grains. One gneiss sample (QL18) contains strongly pleochroic hastingsite, and several samples also contain trace rutile, biotite, paragonite, or porphyroblastic kyanite. One quartzite contains 5–10 mm randomly oriented lath-shaped pseudomorphs (former lawsonite?) containing albite (~45 vol%), muscovite (~15 vol%), and strongly zoned epidote (~40 vol%). Inclusions of coesite and coesite pseudomorphs in kyanite from nearby quartzites (Zhang et al. 2002) indicate that the metasediments and eclogites re-equilibrated at similar depths.

Mineral chemistry

Mineral chemistry was determined with an automated JEOL 733A electron microprobe at Stanford University with operating conditions of 15 nA beam current, and 15 keV accelerating potential, calibrated on natural mineral standards. Raw counts were collected for 20 s and converted to oxide wt% by the CITZAF correction procedure. Minerals were analyzed with a focused (<2 μm) beam, except for micas and talc, for which a 10 μm spot was used. Representative mineral compositions are listed in Table 2.

Garnet

Eclogitic garnets contain low Grs with nearly equal amounts of Prp and Alm components (Fig. 5), and low (<1 wt%) MnO. Most garnets show little or no zoning, but several grains contain inclusions of paragonite and Amp I within an Fe-richer inner zone (Table 2a, analysis 2), surrounded by an outer, Mg-richer zone (Table 2a, analysis 3) interpreted to represent a second stage of garnet growth under eclogite-facies conditions. Garnet in gneiss is spessartine-rich (15–20 wt% MnO).

Epidote

Epidote poikiloblasts (Ep II and Ep III) in fresh eclogites contain $X_{Fe} = 0.15–0.18$ [$X_{Fe} = Fe/(Fe + Al)$, all Fe assumed Fe^{3+}; Fig. 6; Table 2b, analyses 1, 2, 6, 8]; the compositions of the poikiloblastic epidotes are similar in different samples, although one epidote lath (Ep I/II?) that contains a compound inclusion of talc + phengite has an Fe-poor medial zone (Figs. 4c and 6; Table 2b, analysis 7). Inclusion (Ep I) and retrograde (Ep IV) grains contain up to $X_{Fe} = 0.27$ (Fig. 6; Table 2b, analyses 4 and 5). Low Ca pfu may indicate Sr or REE substitution (Fig. 6). These elements were not analyzed in this study, but Nagasaki and Enami (1998) report that Sr-bearing epidote is common throughout the Sulu terrane, but that retrograde epidote is Sr-poor. The Ca-deficiency in Ep I-III analyses and its near absence in the Ep IV analyses (Fig. 6) may reflect a compositional pattern similar to that observed by Nagasaki and Enami (1998). Skeletal epidote in gneiss and quartzite is zoned, with $X_{Fe} = 0.13$ cores surrounded by thin rims with $X_{Fe} = 0.31$ and up to 1 wt% MnO* (total Mn reported as MnO; Table 2b, analysis 3).

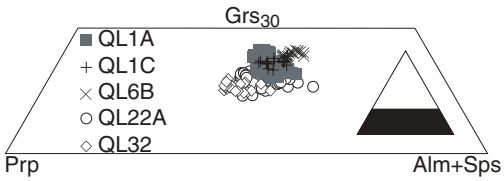

FIGURE 5. Eclogite garnet compositions.

TABLE 2C. Eclogite clinopyroxene compositions

Sample	QL1A-sym	QL32-c	QL32-r	QL6B
Analysis	1	2	3	4
SiO_2	54.41	56.04	56.16	57.19
TiO_2	–	0.08	–	0.06
Al_2O_3	3.42	8.72	8.80	13.81
Cr_2O_3	–	–	–	0.05
Fe_2O_3	1.68	5.24	4.53	–
FeO	5.03	3.31	3.46	2.94
MgO	12.82	7.93	8.07	7.20
CaO	21.02	11.94	12.12	10.81
Na_2O	2.21	7.41	7.28	8.35
Totals	100.59	100.67	100.44	100.41
Si	1.982	2.000	2.006	1.997
Ti	–	0.002	–	0.002
Al	0.147	0.367	0.371	0.569
Cr	–	–	–	0.001
Fe^{3+}	0.046	0.141	0.122	–
Fe^{2+}	0.153	0.099	0.103	0.086
Mg	0.696	0.422	0.430	0.375
Ca	0.820	0.457	0.464	0.404
Na	0.156	0.513	0.505	0.566
Sum	4.000	4.000	4.000	3.999

Notes: Formulae calculated for 6 O atoms. Abbreviations: c = core; r = rim; sym = symplectite.

TABLE 2D. Eclogite amphibole compositions

Sample	QL1C-r	QL3-i	QL6B	QL32
Note	Amp III	Amp I		Amp II
Analysis	1	2	3	4
SiO_2	40.08	42.74	48.48	55.93
TiO_2	0.37	–	0.17	–
Al_2O_3	15.58	16.70	13.80	6.15
Fe_2O_3	3.67	3.23	1.39	3.13
FeO	11.53	8.13	7.38	2.86
MnO	0.15	0.07	–	–
MgO	10.56	11.92	13.54	19.99
CaO	10.74	8.80	7.75	7.94
Na_2O	3.23	4.25	4.75	3.36
K_2O	1.06	0.40	0.45	0.10
Totals	96.98	96.25	97.70	99.47
Si	6.015	6.258	6.852	7.554
Ti	0.042	–	0.018	–
Al	2.757	2.883	2.300	0.979
Fe^{3+}	0.415	0.356	0.147	0.319
Fe^{2+}	1.448	0.996	0.872	0.323
Mn	0.020	0.009	–	–
Mg	2.362	2.601	2.852	4.024
Ca	1.727	1.381	1.173	1.150
Na	0.941	1.205	1.302	0.880
K	0.203	0.075	0.081	0.017
Sum	15.929	15.763	15.598	15.245

Notes: Formulae calculated for 23 O atoms. Abbreviations: c = core; r = rim; i = inclusion.

Omphacite

Omphacites from kyanite, quartz, and epidote-free eclogite QL6B do not contain any Acm component, whereas all other omphacites are calculated to contain 5 to 20 mol% Acm (Fig. 7a; Table 2c). All compositions lie within the omphacite field defined by Morimoto et al. (1988). Contents of Fe^{3+} were estimated by the charge-balance recalculation technique of Droop (1987), but temperature overestimation by the Grt-Omp thermometer (see *P-T* section below) indicates that ferric iron in omphacite is probably significantly underestimated. Omphacites are zoned, with homogeneous, Jd- and Acm-rich cores surrounded by slightly Na-poorer rims (Fig. 7b; Table 2c, analyses 2 and 3). The idioblastic shape of some optical cores suggests that the zoning is the result of primary growth rather than retrograde diffusion.

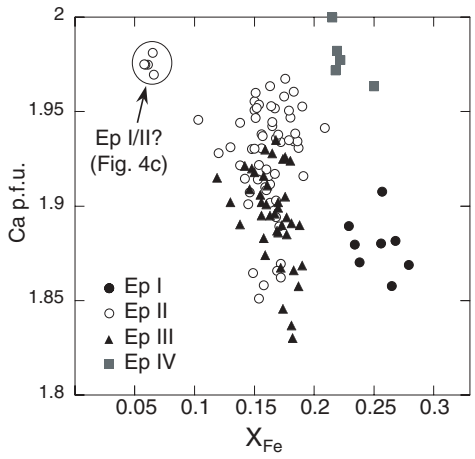

FIGURE 6. Eclogite epidote compositions [$X_{Fe} = Fe/(Fe + Al)$; all iron assumed ferric]. Most epidote poikiloblasts (Ep II + Ep III) have $X_{Fe} = 0.15–0.18$, and are variably low in Ca, which may be related to Sr or REE (not analyzed). The Fe-poor medial region of a grain (Ep I/II?) containing a Phe + Tlc inclusion (see Fig. 4c) contains the lowest analyzed X_{Fe}; the Fe-richer core and rim of this grain are similar to the poikiloblast compositions. Both Ep I and Ep IV are Fe-rich ($X_{Fe} = 0.20–0.27$), but Ep IV is much less deficient in Ca.

TABLE 2E. Eclogite phengite, paragonite, and talc compositions

Sample	QL6B-c	QL6B-r	QL32-c	QL32-r	QL3-i	QL32	QL32-c	QL32-r
Min	Phe	Phe	Phe	Phe	Pg	Pg	Tlc	Tlc
Analysis	1	2	3	4	5	6	7	8
SiO_2	54.10	52.41	51.72	51.07	46.83	46.07	62.35	61.67
TiO_2	0.19	0.31	0.22	0.31	–	–	–	–
Al_2O_3	22.30	25.39	22.97	23.90	38.83	38.54	0.51	1.19
Cr_2O_3	–	–	–	0.07	–	–	–	–
Fe_2O_3	–	–	–	–	–	–	0.27	–
FeO	1.35	1.72	2.11	2.29	1.05	0.69	2.58	2.71
MnO	–	–	–	–	0.10	–	–	–
MgO	5.55	4.48	4.88	4.40	0.21	0.21	29.65	28.54
CaO	–	–	–	–	0.26	0.35	–	–
Na_2O	0.13	0.60	0.15	0.32	6.26	7.12	0.09	0.10
K_2O	10.92	9.95	10.64	10.45	1.62	0.80	–	0.17
Totals	94.55	94.86	92.70	92.82	95.16	93.78	95.44	94.38
Si	3.619	3.489	3.548	3.502	3.013	2.999	3.980	3.98
Ti	0.010	0.015	0.011	0.016	–	–	–	–
Al	1.759	1.993	1.858	1.932	2.945	2.958	0.038	0.091
Cr	–	–	–	0.004	–	–	–	–
Fe^{3+}	–	–	–	–	–	–	0.013	–
Fe^{2+}	0.076	0.095	0.121	0.131	0.056	0.038	0.138	0.146
Mn	–	–	–	–	0.005	–	–	–
Mg	0.553	0.445	0.498	0.450	0.020	0.021	2.821	2.745
Ca	–	–	–	–	0.018	0.024	–	–
Na	0.016	0.077	0.021	0.043	0.781	0.898	0.011	0.013
K	0.933	0.846	0.932	0.915	0.133	0.066	–	0.014
Sum	6.966	6.961	6.989	6.993	6.972	7.004	7.000	6.988

Notes: Formulae calculated for 11 O atoms. Abbreviations: c = core; r = rim; i = inclusion.

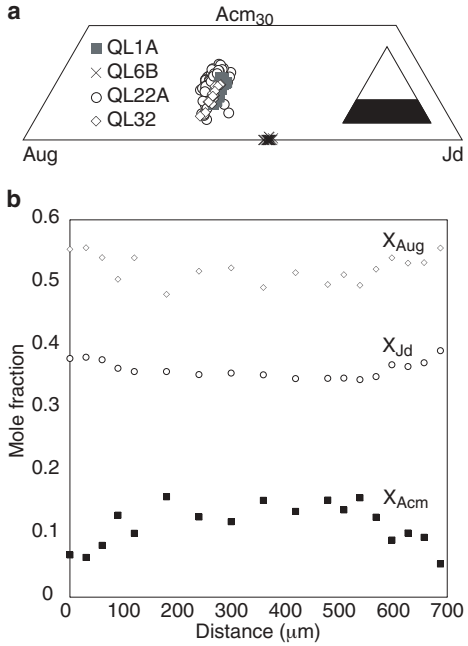

FIGURE 7. (**a**) Omphacite compositions; (**b**) Omphacite zoning profile (sample QL22A); ferric iron calculated using the Droop (1987) technique.

Amphibole

Nomenclature and Fe^{3+} estimates (average of maximum and minimum constraints) follow Leake et al. (1997); amphibole compositions are plotted in Figure 8. Three main stages of amphibole are recognized in the Qinglongshan samples. Amp I is preserved as inclusions in garnet, some as compound inclusions with paragonite ± epidote (Figs. 4a and 4b). Na_B is 0.48–0.53, so analyses plot in both the magnesiotaramite and pargasite fields (Figs. 8a and 8b; Table 2d, analysis 2). Amp II poikiloblasts (barroisite to winchite), which replace talc and omphacite, are the volumetrically dominant amphibole in most samples (Figs. 3c, 4d, and 4e). Amp II is zoned adjacent to talc and omphacite, and is richest in Si, Mg, and Fe^{3+} adjacent to talc (Fig. 8c). Amp III (magnesiohornblende to pargasite; Na_B is 0.22–0.44, most analyses ~0.3) is present only in extensively amphibolitized samples, and contains higher K_2O than other amphiboles (Table 2d, analysis 1). Amp III rims surrounding Amp II are zoned from magnesiohornblende interiors to pargasite rims (Fig. 8b). Amphibole (with plagioclase and sodic augite) is also present in fine-grained symplectite around garnet and omphacite, but few grains are large enough to analyze. The composition of the symplectite amphibole is similar to the Amp III pargasite; the four low Si (6.2–5.8 Si pfu) and low Mg/(Mg + Fe^{2+}) analyses of sample QL1A represent symplectite amphibole (Figs. 8a–8c). Minor amphibole (magnesiokatophorite) also occurs in Qtz, Ky, Tlc, Ep-free eclogite QL6B; the relation of this amphibole to the distinct stages present in other samples is unclear, although its composition is similar to the barroisite poikiloblasts (Figs. 8a and 8c; Table 2d, analysis 3). Amphibole in gneiss is Si-poor (6.3–6.4 Si pfu), Fe-rich [Mg/(Mg + Fe^{2+}) = 0.32–0.35], and contains ~2 wt% K_2O.

Mica

Phengite in eclogite is zoned from cores with up to 3.6 Si pfu (11 O atom basis) to rims with 3.2–3.5 Si pfu (Fig. 9; Table 2e, analyses 1–4). Phengite Mg/(Mg + Fe) is 0.72–0.84 for most samples, except in sample QL6B [Mg/(Mg + Fe) = 0.81–0.88]. Higher Mg/(Mg + Fe) corresponds to higher Si pfu. Phengite included with talc in epidote (Fig. 4c) contains ~1.3 wt% Na_2O, and one paragonite included with amphibole and epidote in garnet

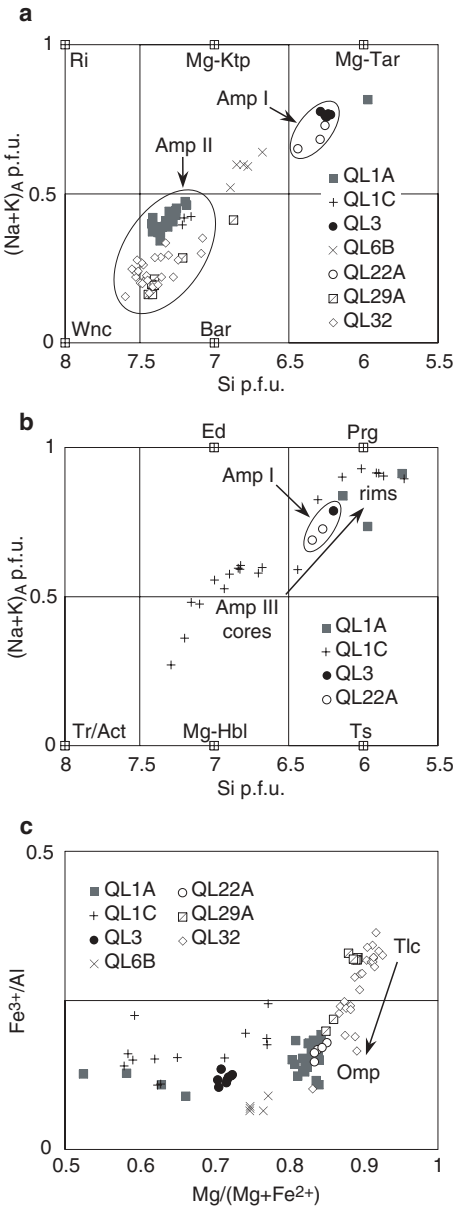

FIGURE 8. Amphibole compositions. Names, formula calculation, and ferric iron estimation follow Leake et al. (1997). (**a**) Sodic-calcic amphibole compositions ($0.5 \leq Na_B \leq 1.5$). (**b**) Calcic amphibole compositions ($Na_B < 0.5$). (**c**) Fe^{3+}/Al vs. $Mg/(Mg + Fe^{2+})$. Sample QL32 is zoned from winchite [high Si, $Mg/(Mg + Fe^{2+})$, Fe^{3+}/Al, and lower A site occupancy] adjacent to talc to barroisite [lower Si, $Mg/(Mg + Fe^{2+})$, Fe^{3+}/Al, higher A site occupancy] adjacent to omphacite. Compositions of amphibole replacing talc + omphacite (Amp II) cluster in the Wnc + Bar fields. Amphibole inclusion (Amp I) compositions cluster in the Mg-Tar and Prg fields (Na_B close to 0.5). Amp III is represented by sample QL1C, and is magnesiohornblende to pargsite ($Na_B = 0.22–0.44$). Symplectite amphibole is represented by the four low-Si (Si pfu = 6.2–5.8) and low $Mg/(Mg + Fe^{2+})$ analyses of sample QL1A. Abbreviations after Kretz (1983), except: Ri, richterite; Mg-Ktp, magnesiokatophorite; Mg-Tar, magnesiotaramite; Wnc, winchite; Bar, barroisite; Mg-Hbl, magnesiohornblende.

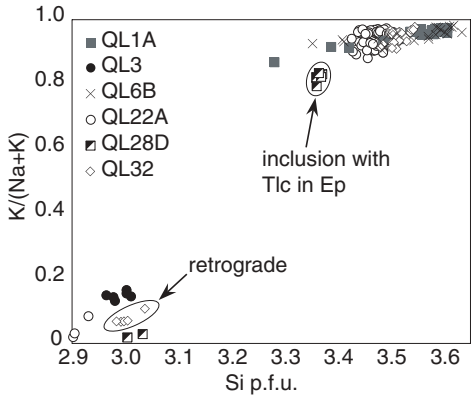

FIGURE 9. Eclogite mica compositions (11 O atom basis). The retrograde paragonite in sample QL32 is shown in Figure 4d; the phengite inclusion in sample QL28D is shown in Figure 4c.

contains ~1.6 wt% K_2O (Fig. 9; Table 2e, analysis 5). Muscovite in gneiss and quartzite contains 3.0–3.2 Si pfu.

Talc

Talc contains low Fe [$Mg/(Mg + Fe^{2+}) = 0.95–0.96$] and Al (0.04–0.09 pfu 11 O atom basis). Talc is zoned from Al, Fe-poor cores to slightly Al, Fe-richer rims adjacent to barroisite (Table 2e, analyses 7 and 8). Talc lacking an amphibole rim is included in epidote (Fig. 4c) and is compositionally identical to matrix talc. The low Al content of talc is consistent with growth at high pressures and low temperatures according to the MASH calculations of Massonne (1995, Fig. 2.3) and the CMASH experiments of Hoschek (1995), which, although at lower pressures, and in the presence of amphibole, showed that lower Al in talc corresponds to higher pressures.

Other minerals

Symplectite around omphacite contains oligoclase ($Ab_{76}An_{23}$), and extensively amphibolitized samples contain larger albite ($Ab_{92}An_8$) grains. Gneissic samples contain two feldspars, $Ab_{98}An_1$ and Ab_5Or_{95}. Titanite in gneiss contains 3.5–4.5 wt% Al_2O_3, and opaque phases in gneiss are Ti-hematite with minor exsolved ferrian ilmenite (Fig. 10).

PETROGENETIC GRID, *P-T* ESTIMATES, AND PROPOSED *P-T* PATH OF THE QINGLONGSHAN ECLOGITES

Fresh eclogite samples QL1A, QL6B, QL22A, and QL32 were selected for *P-T* estimation. Four stages have been recognized, and the paragenesis of each stage is summarized in Figure 11, and a *P-T* diagram is shown in Figure 12. Reactions determined from experimental studies on model systems were used to constrain the *P-T* conditions of the eclogites, combined with thermobarometry (described below) and a petrogenetic grid calculated from mineral rim compositions of sample QL32 to constrain the peak and early retrograde conditions (stages II and III, with partial constraint for stage IV).

I. Prograde stage

Paragonite + Amp I + Ep I inclusions in the Fe-richer inner region of garnets provide the earliest record of the prograde

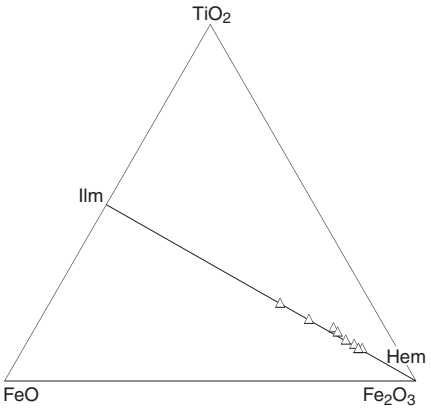

FIGURE 10. Compositions of Fe-Ti oxide from gneiss sample QL1B. Ferric iron estimated by the Droop (1987) recalculation technique.

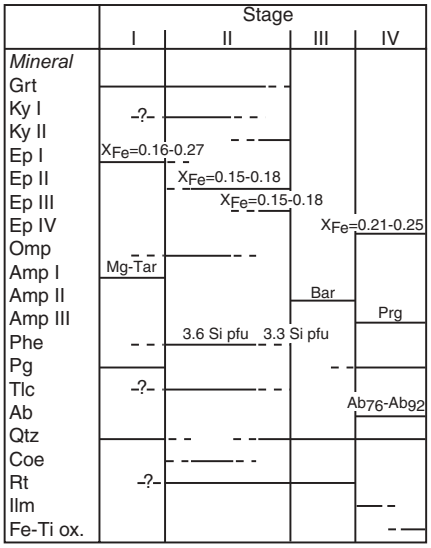

FIGURE 11. Paragenetic diagram for epidote eclogites. Stages I-IV are discussed in the text.

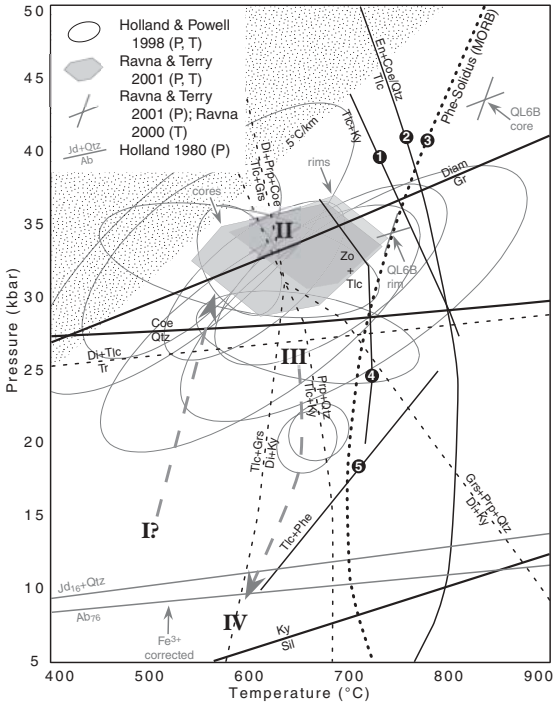

FIGURE 12. *P-T* grid and *P-T* estimates. Polymorphic phase transitions are shown in bold (calculated with the THERMOCALC v3.1 program and data set of Holland and Powell 1998). The uncertainty in *P-T* estimates calculated by THERMOCALC is indicated by the size of the ellipse (1σ); uncertainty in Ravna and Terry (2001) estimates is approximately ±65 °C, ±3.2 kbar (E.J.K. Ravna, pers. commun. 2003). The stippled area corresponds to geothermal gradients less than 5°C/km. Key to numbered reactions: 1 = Tlc+Ky = Prp in MASH, calculated by Massonne (1995); 2 = talc dehydration experimentally determined in the talc + H_2O system (Pawley and Wood 1995); 3 = experimentally determined phengite solidus in MORB (Poli and Schmidt 1998; Schmidt 1996); 4 = Zo + Tlc stability experimentally determined in KCMASH (Hermann 2002); 5 = Tlc + Phe = Phl + Ky + Qtz + H_2O experimentally determined in KMASH (Massonne and Schreyer 1989). The light dashed lines show the petrogenetic grid reactions calculated using the data set of Holland and Powell (1998) and mineral rim compositions from sample QL32, assuming unit H_2O activity. The heavy dashed gray line is the proposed *P-T* path of the Qinglongshan eclogites; Roman numerals refer to the stages discussed in the text and in Figure 11. Abbreviations follow Kretz (1983) except Diam (diamond), Coe (coesite), and Phe (phengite).

path. *P-T* conditions of this stage are poorly constrained, but must lie within the paragonite and amphibole stability fields. The temperature is unconstrained, but based on experimental studies (see below), the pressure is probably 12–22 kbar. A chlorite inclusion in one sample may be part of the prograde assemblage, but a secondary origin cannot be excluded. Foliation defined by omphacite and phengite formed during this stage. Experiments on MORB (Schmidt and Poli 1998) indicate that paragonite forms at P = 12–16 kbar (at T = 500–650 °C) and breaks down at ~22 kbar (at T = 500–700 °C). This reaction is responsible for the first appearance of kyanite in MORB (Poli and Schmidt 1995), and may be responsible for the growth of Ky I. Experimental studies of amphibole breakdown (e.g., Ernst and Liu 1998; Schmidt and Poli 1998; Liu et al. 1996; Poli and Schmidt 1995; Thompson and Ellis 1994) have demonstrated that in basaltic bulk compositions, aluminous amphibole breakdown is highly pressure dependent, and occurs at 22–25 kbar. The experiments of Thompson and Ellis (1994) in the CMASH system showed that amphibole + quartz can produce talc + kyanite + zoisite + clinopyroxene. An analogous reaction may be responsible for the appearance of Ep II + talc in the Qinglongshan samples, although reported Qinglongshan bulk compositions (see Table 2 of Zhang et al. 1995a) indicate slightly higher SiO_2, much higher Fe_2O_3 (~2×), lower MgO (0.6–0.8×) and lower CaO (0.7–0.8×) relative to MORB (see Table 1 of Ernst and Liu 1998).

Schertl et al. (1991, p. 20) raised the question of how inclusions such as paragonite can be preserved in refractory phases even though the matrix of the rock experienced *P-T* conditions beyond the stability field of the enclosed mineral, and they suggested that the host mineral may have acted as a "pressure vessel" around the inclusion. As shown by elastic models of host-inclusion mineral pairs (e.g., Rosenfeld and Chase 1961; Zhang

TABLE 3. *P-T* estimates

Sample		Holland and Powell 1998 *P* (kbar), *T* (°C)	Ravna and Terry 2001 *P* (kbar), *T* (°C)	Ravna 2000 *T* (°C) stoichiometry	Ravna 2000 *T* (°C) Fe^{3+} = Na-Al-Cr
Ql1a	core	*33.4±6.6, 545±107	32.6, 541	791	710
	rim	32.5±4.4, 533±66	34.6, 578	854	765
QL6B	core	32.6±2.6, 591±93	43.5, –	835	835
	rim	27.3±2.1, 660±74	34.4, –	742	742
QL22A, Grt 1	core	27.9±5.6, 612±106	28.7, 616	715	804
Grt 2	core	30.3±5.8, 706±115	33.0, 725	861	983
	rim	–,–	31.0, 688	831	918
Grt 3	core	*31.2±3.6, 606±60	32.7, 628	853	843
	rim	*31.6±4.1, 683±77	34.8, 725	995	987
QL32, Grt 1	core	32.6±2.5, 591±28	36.4, 676	964	945
	rim	20.8±1.3, 671±20	34.7, 706	965	910
Grt 2	core	–,–	35.4, 649	900	884
	rim	20.1±1.4, 659±20	33.7, 677	901	852

Notes: Reactions used for the Holland and Powell (1998) estimates are listed in the deposit items.[1]
* Incomplete set of reactions.

1998), the difference in compressibility and thermal expansivity between host and inclusion will generally result in an inclusion pressure different from the external pressure. Inclusions (such as paragonite or amphibole) that are significantly more compressible than the garnet host will experience pressures lower than the external pressure for pressures higher that the entrapment pressure, and therefore may remain within their stability fields.

II. Peak stage

The peak stage is represented by garnet, omphacite, phengite, rutile, epidote, kyanite, talc, and coesite. Coesite pseudomorphs are present in garnet, omphacite, and epidote (Figs. 3a and 3b). *P-T* estimates based on mineral rim compositions overlap estimates based on core compositions. The preferred peak stage conditions are 30–35 kbar, 600–700 °C, determined by the THERMOCALC v3.1 program and data set (Holland and Powell 1998) and the Ravna and Terry (2001) thermobarometer (*P-T* results summarized in Table 3). The Ravna and Terry (2001) thermobarometer employs the following reactions:

$$3Di + 2Ky = Grs + Prp + 2Qtz/Coe \quad (1)$$
$$Prp + 3Ms + Qtz/Coe = 3Cel + 4Ky \quad (2)$$
$$6Di + 3Ms = 2Grs + Prp + 3Cel \quad (3)$$

where Cel denotes the celadonite component of phengite. For the THERMOCALC results listed in Table 3 (reactions listed in the deposit items)[1], activities were calculated using the *a-X* program of Holland and Powell (1998), and unit H_2O activity was assumed. Reduction of the assumed H_2O activity to 0.5 results in a 30–50 °C reduction in temperature and 1.5–2.5 kbar reduction in pressure, which is within the uncertainty of the calculations. The Grt-Omp Fe^{2+}-Mg thermometer (Ravna 2000) yields unreasonably high temperatures (Table 3; see discussion section). Sample QL6B lacks kyanite and quartz, so temperature estimates rely on reaction 3 (above) and the Grt-Omp Fe^{2+}-Mg exchange thermometer (Ravna 2000), and thus conditions may be overestimated for this sample also. The maximum temperature permissible for the Qinglongshan eclogites is limited by the stability of talc on its own bulk composition, which is no higher than 800–820 °C (Pawley and Wood 1995). The preservation of talc in kyanite (with minor Amp II rim, Fig. 4c) indicates that the Tlc + Ky = Prp + Qtz/Coe dehydration reaction was not significantly overstepped during metamorphism, thus constraining the *P-T* path to relatively low temperature. This reaction is calculated for rim compositions of sample QL32 (light dashed line in Fig. 12), and for the MASH system (sold line 1, calculated by Massonne 1995). An additional constraint on the peak temperature permissible for these samples is the phengite solidus for MORB (Poli and Schmidt 1998; Schmidt 1996). Although reduced H_2O activity will shift the incongruent melting of phengite to higher temperature, and Qinglongshan bulk compositions are different from MORB, dehydration reactions involving talc, epidote, and phengite will occur at lower temperatures. Experiments by Hermann (2002) on a continental crust bulk composition located the Tlc + Phe, Tlc + Ky, and Tlc + Zo dehydration reactions at temperatures below 720–750 °C; the lower Prp content of eclogitic garnets compared with the KCMASH system should reduce the maximum temperature stability of talc, but Fe^{3+} will stabilize epidote to higher temperatures.

III. Early retrograde stage

Ep III and Ky II poikiloblasts grew, and talc + omphacite (±minor garnet and kyanite) reacted to form barroisitic amphibole (Amp II) ± quartz (Fig. 4d). On the grid (Fig. 12), the simplified reaction Di + Tlc = Tr (calculated from rim compositions of sample QL32) occurs slightly below the coesite-quartz transition. Several samples contain talc rimmed by amphibole, and other samples (except QL6B) contain abundant amphibole of the same composition and appearance that locally pseudomorphs the habit of talc. The preservation of talc within kyanite (Fig. 4e) indicates that the Tlc + Ky = Prp + Qtz + H_2O reaction has not been overstepped. On the grid, this reaction occurs at approximately 650–700 °C (calculated from rim compositions of sample QL32). The presence of hydroxl-rich topaz, with X_{OH}~0.35 (Zhang et al. 2002), in the nearby Fushan kyanite quartzites (approximately 3 km south of the study area) further constrains the maximum

[1]For a copy of the deposit items, document item AM-04-073, contact the Business Office of the Mineralogical Society of America (see inside front cover of recent issue) for price information. Deposit items are available on the American Mineralogist web site at http://www.minsocam.org (or contact MSA Business Office for updated link information).

temperature during decompression if these two localities are assumed to be structurally continuous, as oxygen isotope studies seem to indicate (Rumble et al. 2002).

IV. Amphibolite-facies retrogression

Plagioclase + amphibole + sodic augite symplectite, and growth of paragonite, albite, high-Fe epidote, and Amp III (magnesiohornblende to pargasite) indicates an amphibolite-facies overprint. The pressure at which the symplectite formed is constrained to P = 9–11 kbar (at T = 600 °C) by the Ab = Jd + Qtz barometer (Holland 1980), calculated with compositions from sample QL1A, both with and without a Fe^{3+} correction for pyroxene (Fig. 12). The temperature is not constrained quantitatively, but the presence of oligoclase + pargasite in symplectite suggests amphibolite-facies temperatures, and growth of aluminous amphibole (Amp III) also suggests that the temperature remained relatively high at this stage, consistent with adiabatic decompression. The albite + epidote (Ep IV) + amphibole (Amp III) assemblage in extensively retrogressed samples indicates epidote-amphibolite-facies conditions, so stage IV is drawn at the boundary of the amphibolite-facies and epidote-amphibolite-facies (approximately 600 °C, as delimited by Spear 1995). Rutile is partially replaced by an Fe-Ti oxide intergrowth.

Oxygen fugacity conditions

The f_{O_2} during eclogite-facies metamorphism was estimated using the reaction:

$$12Ca_2FeAl_2Si_3O_{12}(OH) = 8Ca_3Al_2Si_3O_{12} + 4Fe_3Al_2Si_3O_{12} + 3O_2 + 6H_2O$$

epidote (X_{Fe} = 0.33) grossular almandine fluid

calculated with the THERMOCALC v.2.5 program and data set of Holland and Powell (1990). Mineral activities were calculated from rim compositions of peak-stage garnet and epidote (Ep II) using the *a-X* program of Holland and Powell (1998); unit H_2O activity was assumed. Reduction of the assumed H_2O activity to 0.8 results in a 7 °C reduction in temperature at $\log f_{O_2} = -10$. At an H_2O activity less than 0.75, epidote is calculated to be unstable over the calculated temperature interval relative to a Grs + Coe + Ky + Hem + H_2O assemblage. However, due to the shallow *P-T* slope of this reaction, temperature uncertainty of this reaction is calculated to be very large (±370 °C), thus limiting its use as a constraint on T and H_2O activity. The results indicate consistent, oxidized conditions for three eclogite samples, approximately 2.5 $\log f_{O_2}$ units above the hematite-magnetite (Hem-Mag) buffer over the calculated temperature range (Fig. 13a). This result is consistent with the Mg-rich compositions of Amp II. Calculations using sample QL32 mineral compositions and the reaction shown in Figure 13b (see discussion section) yield results (not plotted) consistent with those shown in Figure 13a. Conditions were far too oxidizing for the persistence of graphite or the formation of diamond under peak conditions, although *P-T* estimates for several samples lie within the diamond stability field (Fig. 12; Table 3). The graphite-CO_2 (Gr-CO_2) buffer (at X_{CO_2} = 1) is approximately 1 $\log f_{O_2}$ unit below the Hem-Mag buffer (Fig. 13a), and for X_{CO_2} appropriate for epidote stability (<0.04 at P = 30 kbar; see also Boundy et al. 2002), the Gr-CO_2 curve is approximately 1.5 $\log f_{O_2}$ units lower.

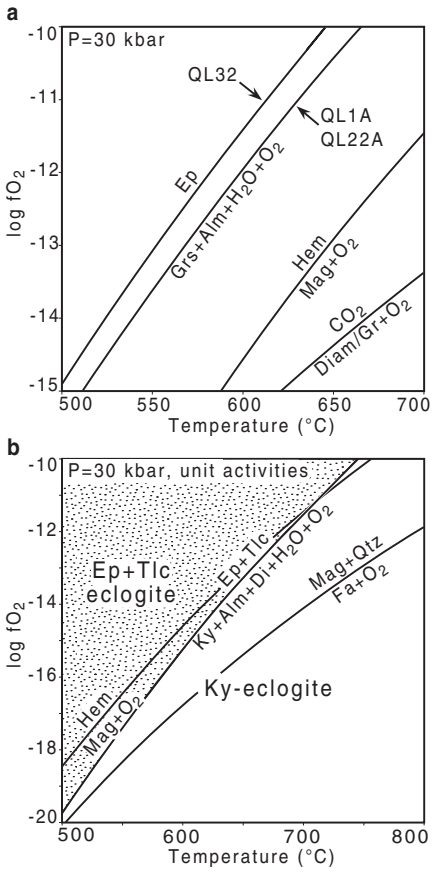

FIGURE 13. Log f_{O_2}-T diagrams calculated with the THERMOCALC v2.5 program and data set of Holland and Powell (1990). (**a**) f_{O_2} estimates for samples QL1A, QL22A, and QL32, calculated from mineral rim compositions. Diamond is stable below 515 °C if f_{O_2} is sufficiently low. (**b**) f_{O_2}-T diagram calculated for unit activities. Ep + Tlc eclogites are the low-temperature, high f_{O_2} equivalents of common kyanite eclogites. The stability field for Ep + Tlc eclogites is stippled.

The presence of Ti-hematite and the absence of magnetite and graphite in gneiss and quartzite samples is consistent with the f_{O_2} calculated for the eclogites. Rim compositions of garnet and epidote in gneiss indicate slightly more oxidized conditions (if calculated at 30 kbar) than eclogitic samples, and compositions of Ti-hematite and garnet included within it indicate f_{O_2} conditions identical to eclogitic Grt-Ep pairs. However, these rocks have thoroughly re-equilibrated at lower pressure (subsolvus alkali feldspar pairs stable) and it is not possible to relate this f_{O_2} estimate to pressure and temperature.

DISCUSSION

The peak pressures estimated in this study are similar to those assumed by Zhang et al. (1995a) but the temperature of 600–700 °C is 80–180 °C lower. The low temperatures obtained in our study are consistent with experimentally determined and calculated stabilities of talc, OH-topaz, and epidote. Temperatures estimated using net-transfer reactions should be less susceptible

to Fe^{3+} estimation uncertainties and later re-equilibration (Ravna and Terry 2001). The high temperatures estimated for Qinglongshan samples by Grt-Cpx Fe^{2+}-Mg exchange thermometry using two Fe^{3+} recalculation schemes [Droop (1987) stoichiometric constraint and $Fe^{3+} = Na - Al - Cr$; Table 3] are inconsistent with experimentally determined mineral stabilities, and may be a result of uncertainties related to Fe^{3+} estimation. Estimation of Fe^{3+} in low-Fe omphacite is especially problematic, because small analytical errors result in large calculated Fe^{3+}/Fe^{2+} variations, resulting in erroneous temperature estimates (Ravna 2000). The preservation of talc in kyanite (with minor Amp II rim, Fig. 4c) indicates that the Tlc + Ky = Prp + Qtz/Coe dehydration reaction was not significantly overstepped during metamorphism, thus constraining the *P-T* path to relatively low temperature.

Eclogites from the northeast Sulu near Weihai contain hypersthene + salite + plagioclase coronas around garnet (Wang et al. 1993; Zhang et al. 1995b), and eclogites near Rongcheng additionally contain corundum-bearing spinel + plagioclase symplectites after kyanite (Nakamura and Hirajima 2000), and paragonite is absent, indicating a granulite-facies overprint. Petrogenetic grid and *P-T* estimates indicate T = 700–850 °C during both peak and granulite-facies stages (near adiabatic decompression; Nakamura and Hirajima 2000). The absence of a granulite-facies overprint in the Qinglongshan samples is consistent with the lower T estimates and the preservation of talc, phengite, epidote, and nearby hydroxyl-rich topaz. The proposed *P-T* path of the Qinglongshan eclogites is consistent with early adiabatic decompression documented in other parts of the Sulu terrane (Carswell and Zhang 2000; Wallis et al. 2000), but the poor temperature constraints of the retrograde stage do not exclude a lower temperature retrograde path.

Donohue and Essene (2000) and Boundy et al. (2002) applied garnet-epidote oxygen barometry to Norwegian eclogite-facies carbonate rocks (580–690 °C, 18–20 kbar), and calculated oxidized conditions 0.3–1.0 log f_{O_2} unit above the hematite-magnetite buffer, suggesting that the oxidized conditions calculated for the Qinglongshan samples are not unreasonable. The garnet-epidote reaction shifts by approximately 0.05 log f_{O_2} unit/kbar relative to the Hem-Mag buffer over the pressure range 1–20 kbar (Donohue and Essene 2000).

Interaction with oxidized, meteoric water in a hydrothermal system such as that hypothesized by Rumble et al. (2002) may be responsible for oxidation and hydration, as well as ^{18}O depletion, of the Qinglongshan epidote-talc eclogite protoliths. If this suggestion is correct, combined oxygen isotope analysis and oxygen fugacity calculation should reveal that the $\delta^{18}O$ of relatively reduced eclogites (such as QL6B) is higher than that of oxidized, Ep + Tlc eclogites. High f_{O_2} may explain the extreme scarcity of microdiamond in this region, despite *P-T* estimates in the diamond stability field. The microdiamond-bearing eclogite (Fig. 1) discovered near Maobei by Xu et al. (2003) must be more reduced than the Qinglongshan samples, and its protolith probably escaped extensive alteration and oxidation during hydrothermal activity. Heterogeneity of hydrothermal alteration combined with lack of extensive fluid flow during UHP metamorphism proposed to explain the preservation of anomalously low, pre-metamorphic isotopic values in this region (Rumble et al. 2002) can also explain the presence of the epidote-free sample QL6B surrounded by epidote + talc eclogites.

The general significance of the Ep + Tlc assemblage in eclogites is illustrated in Figure 13b, which shows the reaction:

$$\underset{\text{talc}}{8Mg_3Si_4O_{10}(OH)_2} + \underset{\text{epidote } (X_{Fe} = 0.33)}{12Ca_2FeAl_2Si_3O_{12}(OH)} =$$
$$\underset{\text{diopside}}{24CaMgSi_2O_6} + \underset{\text{almandine}}{4Fe_3Al_2Si_3O_{12}} + \underset{\text{kyanite}}{8Al_2SiO_5} + \underset{\text{fluid}}{3O_2 + 6H_2O}$$

(calculated for unit activities), and shows that epidote-talc eclogites are low-temperature, oxidized equivalents of the more common kyanite eclogites. As the Qinglongshan samples demonstrate, talc-bearing eclogite assemblages do not necessarily require Mg-rich bulk compositions, as is sometimes stated (e.g., Liou and Zhang 1995). Instead, the high $Mg/(Mg + Fe^{2+})$ needed for talc stability can be generated from rocks with a low $Mg/(Mg + Fe_{Total})$ if sufficient Fe is oxidized to Fe^{3+} and sequestered in Fe^{3+} minerals, such as epidote.

Acknowledgments

This research was supported by the National Science Foundation (NSF EAR0003355 to J.G. Liou), and grants from the Geological Society of America (grant number 7466-03) and the Stanford University McGee Fund to C.G. Mattinson. E.J. Krogh Ravna provided a computer spreadsheet to calculate the Ravna (2000) and Ravna and Terry (2001) thermobarometers. We thank D.K. Bird, W.G. Ernst, and M.O. McWilliams for critical reviews and helpful comments on a preliminary version of this manuscript. The text of this paper was considerably improved by the comments and suggestions of associate editor J. Thompson and reviewers Z. Page and G. Franz.

References cited

Baker, J., Matthews, A., Mattey, D., Rowley, D., and Xue, F. (1997) Fluid-rock interactions during ultra-high pressure metamorphism, Dabie Shan, China. Geochimica et Cosmochimica Acta, 61, 1685–1696.

Boundy, T.M., Donohue, C.L., Essene, E.J., Mezger, K., and Austrheim, H. (2002) Discovery of eclogite facies carbonate rocks from the Lindås Nappe, Caledonides, Western Norway. Journal of Metamorphic Geology, 20, 649–667.

Carswell, D.A. and Zhang, R.Y. (2000) Petrographic characteristics and metamorphic evolution of ultrahigh-pressure eclogites in plate-collision belts. In W.G. Ernst, and J.G. Liou, Eds., Ultra-high pressure metamorphism and geodynamics in collision-type orogenic belts, p. 39–56. Bellwether Publishing, Columbia.

Chopin, C. (1984) Coesite and pure pyrope in high-grade blueschists of the western Alps: a first record and some consequences. Contributions to Mineralogy and Petrology, 86, 107–118.

Donohue, C.L. and Essene, E.J. (2000) An oxygen barometer with the assemblage garnet–epidote. Earth and Planetary Science Letters, 181, 459–472.

Droop, G.T.R. (1987) A general equation for estimating Fe^{3+} concentrations in ferromagnesian silicates and oxides from microprobe analyses, using stoichiometric criteria. Mineralogical Magazine, 51, 431–435.

Enami, M. and Nagasaki, A. (1999) Prograde P-T path of kyanite eclogites from Junan in the Sulu ultrahigh-pressure province, eastern China. The Island Arc, 8, 459–474.

Ernst, W.G. and Liu, J. (1998) Experimental phase-equilibrium study of Al- and Ti-contents of calcic amphibole in MORB–A semiquantitative thermobarometer. American Mineralogist, 83, 952–969.

Ernst, W.G., Maruyama, S., and Wallis, S. (1997) Buoyancy-driven, rapid exhumation of ultrahigh-pressure metamorphosed continental crust. Proceedings of the National Academy of Sciences, U.S.A., 94, 9532–9537.

Grimmer, J.C., Ratschbacher, L., McWilliams, M., Franz, L., Gaitzsch, I., Tichomirowa, M., Hacker, B.R., and Zhang, Y. (2003) When did the ultrahigh-pressure rocks reach the surface? A $^{207}Pb/^{206}Pb$ zircon, $^{40}Ar/^{39}Ar$ white mica, Si-in-white mica, single-grain provenance study of Dabie Shan synorogenic foreland sediments. Chemical Geology, 197, 87–110.

Hacker, B.R., Ratschbacher, L., Webb, L., McWilliams, M.O., Ireland, T., Calvert, A., Dong, S., Wenk, H.-R., and Chateigner, D. (2000) Exhumation of ultrahigh-pressure continental crust in east central China: Late Triassic-Early Jurassic tectonic unroofing. Journal of Geophysical Research, 105(B6), 13339–13364.

Hermann, J. (2002) Experimental constraints on phase relations in subducted continental crust. Contributions to Mineralogy and Petrology, 143, 219–235.

Holland, T.J.B. (1980) The reaction albite = jadeite + quartz determined experimentally in the range 600–1200 °C. American Mineralogist, 65, 129–134.

Holland, T.J.B. and Powell, R. (1990) An internally consistent thermodynamic

data set with uncertainties and correlations: the system Na_2O-K_2O-CaO-MgO-MnO-FeO-Fe_2O_3-Al_2O_3-SiO_2-TiO_2-C-H_2-O_2. Journal of Metamorphic Geology, 8, 89–124.

——— (1998) An internally consistent thermodynamic data set for phases of petrological interest. Journal of Metamorphic Geology, 16, 309–343.

Hoschek, G. (1995) Stability relations and Al content of tremolite and talc in CMASH assemblages with kyanite + zoisite + quartz + H_2O. European Journal of Mineralogy, 7, 353–362.

Katayama, I., Maruyama, S., Parkinson, C.D., Terada, K., and Sano, Y. (2002) Pressure-temperature-time path of the Kokchetav UHP metamorphism deduced from mineral inclusions and SHRIMP geochronology of zircons. In C.D. Parkinson, I. Katayama, J.G. Liou, and S. Maruyama, Eds., The Diamond-Bearing Kokchetav Massif, Kazakhstan, p. 381–395. Universal Academy Press, Tokyo, Japan.

Kretz, R. (1983) Symbols for rock-forming minerals. American Mineralogist, 68, 277–279.

Krogh, E.J. (1982) Metamorphic evolution of Norwegian country-rock eclogites, as deduced from mineral inclusions and compositional zoning in garnets. Lithos, 15, 305–321.

Leake, B.E., Woolley, A.R., Arps, C.E.S., Birch, W.D., Gilbert, M.C., Grice, J.D., Hawthorne, F.C., Kato, A., Kisch, H.J., Krivovichev, V.G., Linthout, K., Laird, J., Mandarino, J.A., Maresch, W.V., Nickel, E.H., Rock, N.M.H., Schumacher, J.C., Smith, D.C., Stephenson, N.C.N., Ungaretti, L., Whittaker, E.J.W., and Youzhi, G. (1997) Nomenclature of amphiboles: Report of the Subcomittee on Amphiboles of the International Mineralogical Association, Commission on New Minerals and Mineral Names. American Mineralogist, 82, 1019–1037.

Liou, J.G. and Zhang, R.Y. (1995) Significance of ultrahigh-P talc-bearing eclogitic assemblages. Mineralogical Magazine, 59, 93–102.

Liou, J.G., Zhang, R.Y., Katayama, I., and Maruyama, S. (2002) Global distribution and petrotectonic characterizations of UHPM terranes. In C.D. Parkinson, I. Katayama, J.G. Liou, and S. Maruyama, Eds. The diamond-bearing Kokchetav massif, Kazakhstan. Universal Academy Press, Tokyo, Japan.

Liu, J., Bohlen, S.R., and Ernst, W.G. (1996) Stability of hydrous phases in subducting oceanic crust. Earth and Planetary Science Letters, 143, 161–171.

Liu, F., Xu, Z., Katayama, I., Yang, J., Maruyama, S., and Liou, J.G. (2001) Mineral inclusions in zircons of para- and orthogneiss from pre-pilot drill hole CCSD-PP1, Chinese Continental Scientific Drilling Project. Lithos, 59, 199–215.

Liu, F., Xu, Z., Liou, J.G., Katayama, I., Masago, H., Maruyama, S., and Yang, J. (2002) Ultrahigh-pressure mineral inclusions in zircons from gneissic core samples of the Chinese Continental Scientific Drilling Site in eastern China. European Journal of Mineralogy, 14, 499–512.

Massonne, H.-J. (1995) Experimental and petrogenetic study of UHPM. In R.G. Coleman, and X. Wang, Eds., Ultrahigh Pressure Metamorphism, p. 33–95. Cambridge University Press, New York.

Massonne, H.-J., and Schreyer, W. (1989) Stability field of the high-pressure assemblage talc + phengite and two new phengite barometers. European Journal of Mineralogy, 1, 391–410.

Massonne, H.-J., and Szpurka, Z. (1997) Themodynamic properties of white micas on the basis of high-pressure experiments in the system K_2O–MgO–Al_2O_3–SiO_2–H_2O and K_2O–FeO–Al_2O_3–SiO_2–H_2O. Lithos, 41, 229–250.

Morimoto, N., Fabries, J., Ferguson, A.K., Ginzburg, I.V., Ross, M., Seifert, F.A., Zussman, J., Aoki, K., and Gottardi, G. (1988) Nomenclature of pyroxenes. American Mineralogist, 73, 1123–1133.

Nagasaki, A., and Enami, M. (1998) Sr-bearing zoisite and epidote in ultra-high pressure (UHP) metamorphic rocks from the Su-Lu province, eastern China: An important Sr reservoir under UHP conditions. American Mineralogist, 83, 240–247.

Nakamura, D., and Hirajima, T. (2000) Granulite-facies overprinting of ultrahigh-pressure metamorphic rocks, northeastern Su-Lu region, eastern China. Journal of Petrology, 41, 563–582.

Pawley, A.R., and Wood, B.J. (1995) The high-pressure stability of talc and 10 Å phase: Potential storage sites for H_2O in subduction zones. American Mineralogist, 80, 998–1003.

Poli, S., and Schmidt, M.W. (1995) H_2O transport and release in subduction zones: Experimental constraints on basaltic and andesitic systems. Journal of Geophysical Research, 100(B11), 22299–22314.

——— (1998) The high-pressure stability of zoisite and phase relationships of zoisite-bearing assemblages. Contributions to Mineralogy and Petrology, 130, 162–175.

Ratschbacher, L., Hacker, B.R., Webb, L.E., McWilliams, M., Ireland, T., Dong, S., Calvert, A., Chateigner, D., and Wenk, H.-R. (2000) Exhumation of the ultrahigh-pressure continental crust in east central China: Cretaceous and Cenozoic unroofing and the Tan-Lu fault. Journal of Geophysical Research, 105, 13303–13338.

Ravna, E.K. (2000) The garnet–clinopyroxene Fe^{2+}–Mg geothermometer: an updated calibration. Journal of Metamorphic Geology, 18, 211–219.

Ravna, E.J.K. and Terry, M.P. (2001) Geothermobarometry of phengite–kyanite–quartz/coesite eclogites. Eleventh Annual V.M. Goldschmidt Conference, LPI Contribution 1088, Abstract no. 3145. Lunar and Planetary Institute, Houston, Texas.

Rosenfeld, J.L. and Chase, A.B. (1961) Pressure and temperature of crystallization from elastic effects around solid inclusions in minerals? American Journal of Science, 259, 519–541.

Rumble, D. and Yui, T.F. (1998) The Qinglongshan oxygen and hydrogen isotope anomaly near Donghai in Jiangsu Province, China. Geochimica et Cosmochimica Acta, 62, 3307–3321.

Rumble, D., Giorgis, D., Ireland, T., Zhang, Z., Xu, H., Yui, T.F., Yang, J., Xu, Z., and Liou, J.G. (2002) Low $\delta^{18}O$ zircons, U-Pb dating, and the age of the Qinglongshan oxygen and hydrogen isotope anomaly near Donghai in Jiangsu Province, China. Geochimica et Cosmochimica Acta, 66, 2299–2306.

Schmidt, M.W. (1996) Experimental constraints on recycling of potassium from subducted oceanic crust. Science, 272, 1927–1930.

Schmidt, M.W. and Poli, S. (1998) Experimentally based water budgets for dehydrating slabs and consequences for arc magma generation. Earth and Planetary Science Letters, 163, 361–379.

Schertl, H.-P., Schreyer, W., and Chopin, C. (1991) The pyrope-coesite rocks and their country rocks at Parigi, Dora Maira Massif, Western Alps: detailed petrography, mineral chemistry and PT-path. Contributions to Mineralogy and Petrology, 108, 1–21.

Smith, D.C. (1984) Coesite in clinopyroxene in the Caledonides and its implications for geodynamics. Nature, 310, 641–644.

Sobolev, N.V. and Shatsky, V.S. (1990) Diamond inclusions in garnets from metamorphic rocks: a new environment for diamond formation. Nature, 343, 742–746.

Spear, F.S. (1995) Metamorphic phase equilibria and pressure-temperature-time paths. 799 p. Monograph, Mineralogical Society of America, Washington, D.C.

Thompson, A.B. and Ellis, D.J. (1994) CaO + MgO + Al_2O_3 + SiO_2 + H_2O to 35 kb: Amphibole, talc, and zoisite dehydration and melting reactions in the silica-excess part of the system and their possible significance in subduction zones, amphibolite melting and magma fractionation. American Journal of Science, 294, 1229–1289.

Wallis, S., Enami, M., and Banno, S. (2000) The Sulu UHP terrane: A review of the petrology and structural geology. In W.G. Ernst, and J.G. Liou, Eds., Ultra-high pressure metamorphism and geodynamics in collision-type orogenic belts, p. 190–204. Bellwether Publishing, Columbia.

Wang, Q., Ishiwatari, A., Zhao, Z., Hirajima, T., Enami, M., Zhai, M., Li, J., and Cong, B.L. (1993) Coesite-bearing granulite retrograded from eclogite in Weihai, eastern China: a preliminary study. European Journal of Mineralogy, 5, 141–152.

Xu, S., Liu, Y., Chen, G., Compagnoni, R., Rolfo, F., He, M., and Liu, H. (2003) New finding of micro-diamonds in eclogites from Dabie-Sulu region in central-eastern China. Chinese Science Bulletin, 48, 988–994.

Ye, K., Liou, J.-B., Cong, B., and Maruyama, S. (2001) Overpressures induced by coesite-quartz transition in zircon. American Mineralogist, 86, 1151–1155.

Yui, T.-F., Rumble, D., and Lo, C.-H. (1995) Unusually low $\delta^{18}O$ ultra-high-pressure metamorphic rocks from the Sulu Terrain, eastern China. Geochimica et Cosmochimica Acta, 59(13), 2859–2864.

Zhang, R.Y. and Liou, J.G. (2000) Exsolution lamellae in minerals from ultra-high-pressure rocks. In W.G. Ernst, and J.G. Liou, Eds., Ultra-high pressure metamorphism and geodynamics in collision-type orogenic belts, p. 216–228. Bellwether Publishing, Columbia.

Zhang, R.-Y., Hirajima, T., Banno, S., Cong, B., and Liou, J.G. (1995a) Petrology of ultrahigh-pressure rocks from the southern Su-Lu region, eastern China. Journal of Metamorphic Geology, 13, 659–675.

Zhang, R.Y., Liou, J.G., and Ernst, W.G. (1995b) Ultrahigh-pressure metamorphism and decompressional P-T paths of eclogites and country rocks from Weihai, eastern China. The Island Arc, 4, 293–309.

Zhang, R.-Y., Liou, J.G., and Shu, J.F. (2002) Hydroxyl-rich topaz in high-pressure and ultrahigh-pressure kyanite quartzites, with retrograde woodhouseite, from the Sulu terrane, eastern China. American Mineralogist, 87, 445–453.

Zhang, Y. (1998) Mechanical and phase equilibria in inclusion—host systems. Earth and Planetary Science Letters, 157, 209–222.

Zheng, Y.-F., Fu, B., Gong, B., and Li, L. (2003) Stable isotope geochemistry of ultrahigh pressure metamorphic rocks from the Dabie-Sulu orogen in China: implications for geodynamics and fluid regime. Earth-Science Reviews, 62, 105–161.

MANUSCRIPT RECEIVED OCTOBER 18, 2003
MANUSCRIPT ACCEPTED JULY 3, 2004
MANUSCRIPT HANDLED BY JENNIFER THOMSON